The Company of Biologists

RESEARCH ARTICLE

Localized translation regulates cell adhesion and transendothelial migration

Jonathan Bergeman[1], Alexia Caillier[1], François Houle[2], Laurence M. Gagné[1] and Marc-Étienne Huot[1,2,*]

ABSTRACT

Epithelial-to-mesenchymal transition (EMT) is a process by which cancer cells gain the ability to leave the primary tumor site and invade surrounding tissues. These metastatic cancer cells can further increase their plasticity by adopting an amoeboid-like morphology, by undergoing mesenchymal-to-amoeboid transition (MAT). We found that adhering cells produce spreading initiation centers (SICs), transient structures that are localized above nascent adhesion complexes, and share common biological and morphological characteristics associated with amoeboid cells. Meanwhile, spreading cells seem to return to a mesenchymal-like morphology. Thus, our results indicate that SIC-induced adhesion recapitulates events that are associated with amoeboid-to-mesenchymal transition (AMT). We found that polyadenylated RNAs are enriched within SICs, blocking their translation decreased adhesion potential of metastatic cells that progressed through EMT. These results point to a so-far-unknown checkpoint that regulates cell adhesion and allows metastatic cells to alter adhesion strength to modulate their dissemination.

KEY WORDS: Spreading initiation centers, SICs, RNA-binding proteins, Focal adhesion, Translation regulation, Invasion, Mesenchymal cells, Epithelial cells, Epithelial-to-mesenchymal transition, EMT, Mesenchymal-to-amoeboid transition, MAT, Amoeboid-to-mesenchymal transition, AMT

INTRODUCTION

Metastasis remains one of the most detrimental aspects of tumor progression that is often used to determine the prognosis. In order to leave the primary tumor site, disseminating cancer cells have to go through a series of transitions affecting cellular plasticity, adhesion, migration and invasion (Fidler, 2003). This mainly occurs when cells undergo an epithelial-to-mesenchymal transition (EMT) (Grunert et al., 2003; Taddei et al., 2013). By adopting a mesenchymal-like morphology, disseminating cancer cells can invade the stroma by remodeling their cytoskeleton and adapting their adhesion capacities in response to the microenvironment (Grunert et al., 2003; Kopfstein and Christofori, 2006). EMT is a complex molecular process and involves the activity of numerous transcription factors (Lander et al., 2011; Mani et al., 2008; Thiery et al., 2009) that modulate cell polarity and the expression of cell–cell adhesion proteins to gain migratory and invasive properties (Sahai and Marshall, 2003).

[1]Centre de Recherche sur le Cancer de l'Université Laval, Faculté de Médecine, Université Laval, Québec, Canada, G1V 0A6. [2]CRCHU de Québec: Hôtel-Dieu de Québec, Québec, Canada G1R 3S3.

*Author for correspondence (marc-etienne.huot@crchuq.ulaval.ca)

M.É.H., 0000-0001-5155-5338

Disseminating cancer cells that undergo EMT can further increase their cytoskeletal plasticity by adopting an amoeboid-like morphology (Sahai and Marshall, 2003; Vial et al., 2003). In contrast to EMT, mesenchymal-to-amoeboid transition (MAT) does not require transcriptional alterations (Sanz-Moreno et al., 2008). Therefore, disseminating cancer cells can rapidly cycle between these two migratory modes in response to extracellular matrix (ECM) composition (Pankova et al., 2010; Schmidt et al., 2009; Taddei et al., 2014). Wheareas mesenchymal invasion relies on proteolysis and ECM remodeling, amoeboid invasion uses intensive blebbing to enable cancer cells to squeeze through the ECM in a leukocyte-like manner (Friedl et al., 2001; Wolf et al., 2003). Amoeboid-based motility is considered to be integrin-independent (Diz-Munoz et al., 2010; Hegerfeldt et al., 2002), allowing cells to loosely adhere to their environment and facilitate their movement.

Amoeboid morphology is reminiscent of newly adhering cells that generate transient bleb-like structures termed spreading initiation centers (SICs) (Andersson et al., 2008; de Hoog et al., 2004; Serrels et al., 2007). SICs form within the cell periphery, directly above nascent adhesion complexes, and gradually disappear as adhesion complexes mature into focal adhesions (de Hoog et al., 2004; Serrels et al., 2007). As SIC-positive cells progress to the spreading phase, they undergo a similar morphological change as cells that are proceeding through the amoeboid-to-mesenchymal transition (AMT).

Stable isotope labeling with amino acids in cell culture (SILAC) analysis identified numerous focal adhesion markers and RNA-binding proteins as potential SIC components (de Hoog et al., 2004). Interestingly, most SIC-bound RNA-binding proteins were also found amongst our previously characterized Sam68 ribonucleoparticles (RNPs) (Huot et al., 2009b). These RNPs were shown to affect both focal adhesion turnover and cellular spreading (Huot et al., 2009a), and have the ability to modulate mRNA translation (Aulas et al., 2015; Huot et al., 2009b; Klein et al., 2013; Mazroui et al., 2002).

Here, we show that polyadenylated mRNAs are present within SICs, and impairment of their translation greatly decreased cellular adhesion and spreading, while forcing the conservation of amoeboid-like morphology. This implies that SIC-bound mRNA translation modulates cell adhesion and/or spreading progression by controlling the expression of proteins that are involved in adhesion stability. Moreover, we found that translational inhibition decreased the adhesion and transendothelial migration potential of mesenchymal-like metastatic cancer cells, which was not the case with cancer cells of low metastatic capacity that express epithelial markers. This suggests that mechanisms regulating SIC metabolism are involved in the adhesion process of cancer cells that progress through EMT, an event associated with increased metastatic potential.

RESULTS

SICs and the maturation of the focal adhesion complex

To study SIC formation and dynamics, we used MRC-5 primary human fibroblasts, a cell line that has previously been used to define

adhesion processes (de Hoog et al., 2004). As seen in time-lapse live cell imaging, SICs are highly dynamic structures that disappear upon initiation of cellular spreading (Movie 1). SICs are rich in adhesion structure elements, such as vinculin and paxillin, while being surrounded by a thin actin sheet (Fig. 1A). These transient structures found in newly adhering cell are linked to the nascent
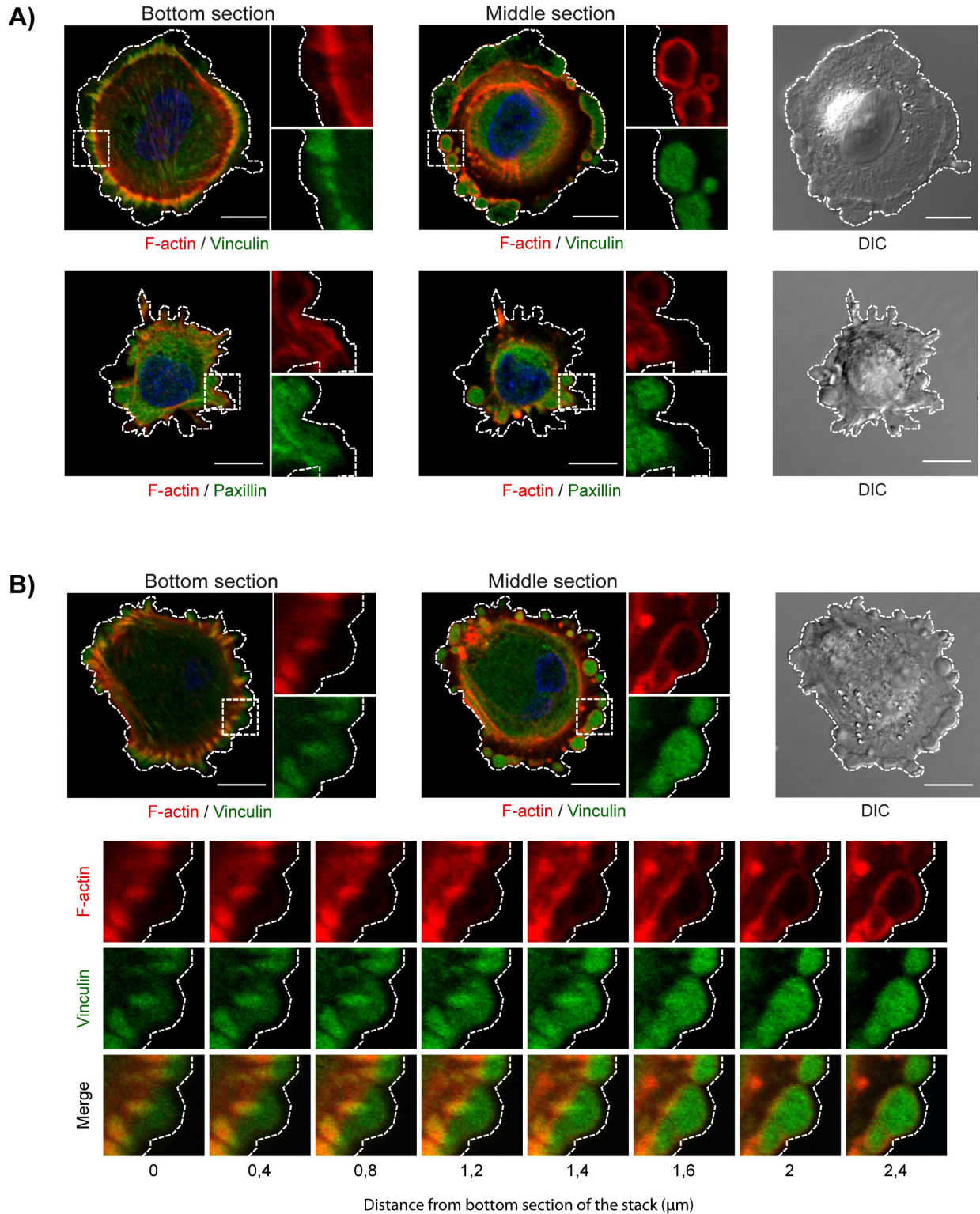

Fig. 1. Spreading initiation centers (SICs) and maturation of the focal adhesion complex. (A) Localization of F-actin (red), vinculin (green) and paxillin (green) in SICs of two adhering MRC-5 cells (one in the upper panels, and a different one in the lower panels). F-actin was detected with CF™568 phalloidin (green). (B) Relative distance between the newly formed focal adhesion complex and SICs. The bottom panel shows the boxed areas from the images above magnified ×2.5. Sequential stack from the lowest to the middle section of a representative confocal stack of an adhering MRC-5 cell, showing vinculin (green) and F-actin (red; by using CF™568 phalloidin) from focal adhesion complex (bottom) and SICs (middle) All scale bars: 10 µm.

adhesion complex and are thought to contribute to focal adhesion site formation and maturation. As seen with vinculin staining, the distance between SICs and adhesion complexes is ~1 µm (Fig. 1B). Although SICs seem to be covering newly formed adhesion complexes, they are closer to the edge of the cell, suggesting that they act as locally compartmentalized storage or sites for manufacture of proteins involved in focal adhesion site formation and maturation.

Localization of RNA-binding proteins within SICs

Our previous work has shown that Sam68 relocalized to near the plasma membrane during cell adhesion (Huot et al., 2009a). This was unexpected considering the nuclear localization of Sam68 at steady-state in fully spread cells (Fig. 2A, upper left panel). Our findings were supported by a study that had used SILAC by listing Sam68 as a potential component of SICs (de Hoog et al., 2004). We therefore determined the presence of Sam68 protein within SICs. As seen in Fig. 2A, Sam68 shows a clear localization within these structures. We also detected the presence of G3BP1 and FMRP, two potential SIC-bound RNA-binding proteins that have also been identified as components of Sam68 RNPs (Huot et al., 2009b). To determine whether these RNA-binding proteins are enriched in SICs, we first assessed the proportion of the passively diffusing green fluorescent protein (GFP) in these structures and compared the average SIC signal with the average cytoplasmic signal (excluding SIC and nuclear signal). This quantification showed that the average GFP signal in SICs corresponds to 40% of the average cytoplasmic signal, suggesting that SIC localization is selective (Fig. 2B). Diffusion-normalized quantification of the RNA-binding protein showed a clear enrichment of Sam68 (260%), G3BP1 (340%) and FMRP (220%) in SICs (Fig. 2C). This secluded enrichment of RNA-binding protein indicates a potential RNA-based control mechanism for SIC metabolism and ensues adhesion consolidation.

To investigate whether Sam68-mediated RNA-binding activity is required for SIC localization, we used two Sam68 mutants defective in RNA binding (G178D and I184N) and compared them with a nuclear localization sequence (NLS) mutant (R436-442A), and a signaling mutant (Y435-440-443F) that had been shown to affect cellular spreading and morphology (Chen et al., 1999; Lukong et al., 2005). Control experiments show that inactivation of either the signaling activity of Sam68 or of its NLS did not modify SIC localization (Fig. 2D). Interestingly, both RNA-binding mutants remained exclusively nuclear during cellular adhesion (Fig. 2D), indicating that Sam68 translocation to SICs is mediated by its association with mRNA.

Localized mRNA translation within SICs

Since the ability of Sam68 to bind mRNA is essential for SIC localization, we investigated the possible presence of mRNA within SICs by using an Alexa-Fluor-596-tagged oligo(dT) probe. This probe successfully stained mRNAs that had colocalized with vinculin – another SIC component (Fig. 3A). Staining was completely abrogated by the addition of competing poly(A) oligonucleotide (Fig. S1A). These results provide the first direct evidence of poly(A) mRNA within SIC structures. Considering that SICs also contain rRNA and multiple RNA-binding proteins that are known to control mRNA translation (de Hoog et al., 2004), we envisioned that localized mRNA translation participated in the formation and maturation of focal adhesion sites. To investigate the impact of translation during the initial phase of adhesion, we treated adhering MRC-5 cells with the general protein synthesis inhibitor cycloheximide (Bennett et al., 1965). For the duration of the adhesion assay, we opted for

cycloheximide treatment at 50 µg ml⁻¹, a concentration that efficiently inhibited translation in all cell lines tested (Fig. S1B), while not affecting cell integrity (Fig. S1C). Cycloheximide treatment provoked a significant increase in SIC numbers within cells (Fig. 3B). Concomitantly, we found that cycloheximide treatment stabilized SIC metabolism throughout early adhesion. Indeed, >60% of cycloheximide-treated adhering cells still produced SICs 2 hours following seeding, whereas less than 30% of untreated cells (mock) presented these structures (Fig. 3C).

The results described above show that inhibition of translation clearly affects SIC metabolism, suggesting the presence of a localized translation within SICs. We assessed this possibility by visualizing translation within SICs after treatment with puromycin – an antibiotic that is incorporated into elongating polypeptides, resulting in the premature release of truncated puromycinylated polypeptides (Schmidt et al., 2009). Although alternative methods could have been used for localized translation visualization (Fallini et al., 2016; Griffin et al., 1998; Halstead et al., 2015), only puromycin incorporation offers a rapid and precise glimpse of translation events, making it a well-suited method to assess translation events in rapid biological processes, such as cell adhesion. Hence, MRC-5 cells were allowed to adhere for 60 min, prior to the addition of 5 µg ml⁻¹ puromycin to the medium 5 min before fixation. Newly synthetized puromycinylated polypeptides were detected by using antibodies directed against puromycin (David et al., 2012; Mardakheh et al., 2015). As seen in Fig. 3D, strong puromycinylation was detected within the adhesion structures of puromycin-treated cells, indicating translational activity within SICs. As expected from their respective effect on translation initiation and elongation, pretreatment with either anisomycin or cycloheximide completely inhibited the incorporation of puromycin (Fig. 3E and Fig. S1D).

While characterizing this translation activity within SICs, we found that translation seemed to be greatly increased in adhering cells as compared to spreading cells (Fig. S2A). To further characterize this elevated translation activity during adhesion, we performed puromycin incorporation assays in MRC-5 cells at different adhering times (Fig. S2B). We found a robust increase of translation in the initial phase of adhesion during the peak of SIC formation (30-60 min), followed by a rapid decrease in puromycin incorporation, corresponding to later phases of SIC maturation (Fig. S2C). These observations prompted us to quantify the relative proportion of translational activity within SICs by measuring SIC-bound puromycinylation in adhering MRC-5 cells. Whole-cell quantification in adhering MRC-5 cells showed that almost 80% of total protein translation was exclusively localized in SICs (Fig. 3F). By quantifying GFP distribution, we determined that the relative cellular volume of SICs is <40% of the total cell volume (Fig. 3G and H).

Although we cannot exclude the contribution of protein translation outside SICs, our results indicate that a large proportion of active translation takes place in these structures during the initial phase of adhesion.

SIC-bound mRNA translation is necessary for correct adhesion in mesenchymal-like cell lines

The results presented above indicate that SIC-localized translation are essential for adhesion consolidation and that blocking translation impairs cell adhesion. By using time-lapse live cell imaging, we observed a significant change in the number of MRC-5 cells that did not proceed to the spreading phase when treated with cycloheximide (Movie 2A and B). Cycloheximide-treated cells kept forming successive waves of SICs and remained stalled at the adhesion phase, unable to consolidate their adhesion and initiate
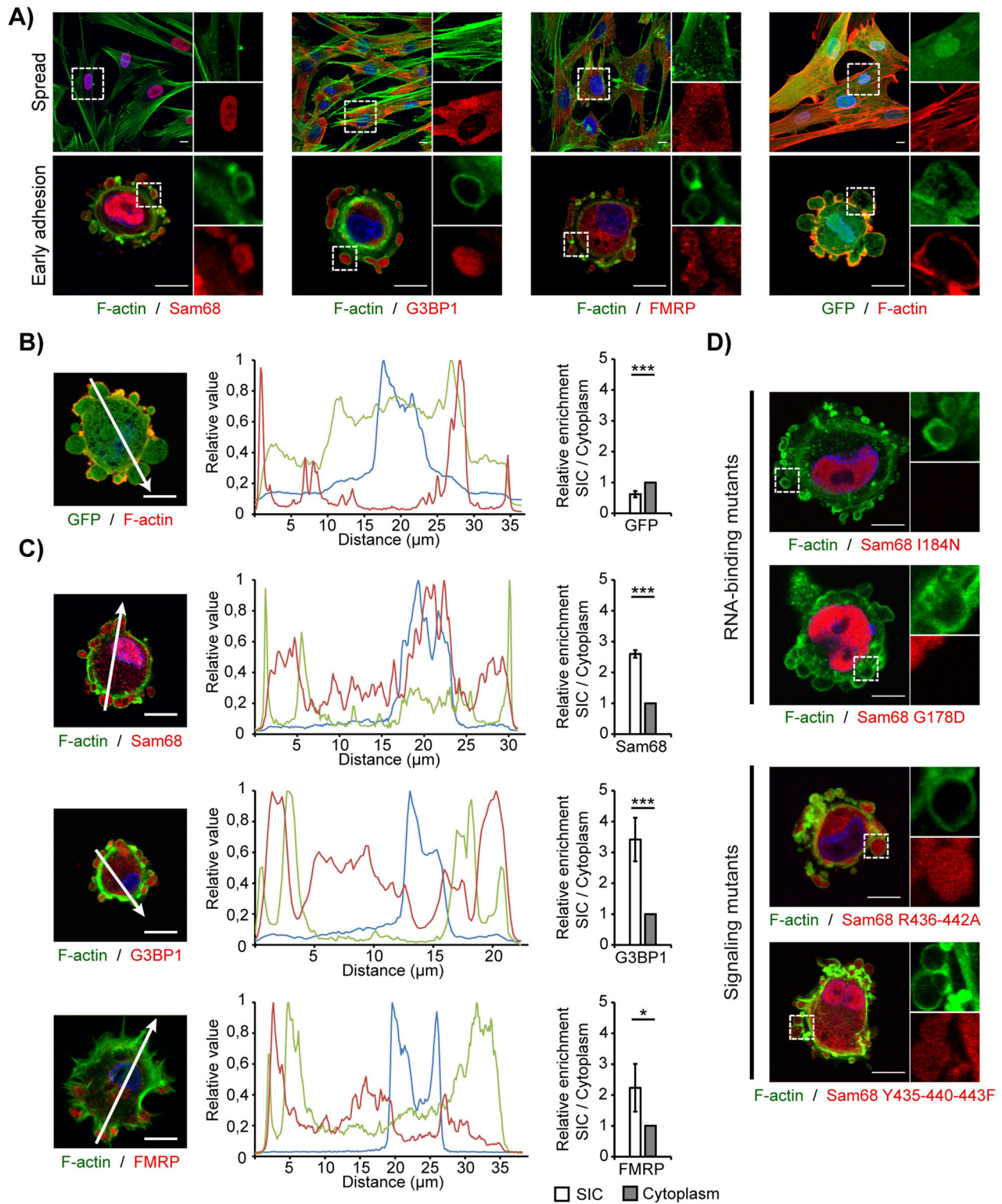
Fig. 2. RNA-binding proteins are enriched within spreading initiation centers (SICs). (A) Representative confocal mid-section plane of Sam68 (red), G3BP1 (red), FMRP (red) and GFP (green) in adhering MRC-5 cells. F-actin was detected with CF™488 phalloidin (green) or CF™568 phalloidin (red). (B) Quantification of the fold-enrichment of GFP in SICs. The graph represents the signal intensity of GFP (green), F-actin (red) and DAPI (blue) following the cell axis (indicated by a white arrow) on a representative adhering MRC-5 cell (left panel). Relative quantification of the SIC enrichment of GFP in ten different cells collected from three different experiments. Error bar represent±s.d.; ***$P \leq 0.001$ (two-tailed t-test). (C) Quantification of the fold-enrichment of RNA-binding proteins in SICs. The graphs represent the signal intensity of Sam68 (red; top graph), G3BP1 (red; middle graph), FMRP (red; bottom graph), F-actin (green) and DAPI (blue) following the cell axis (indicated by a white arrow) on representative adhering MRC-5 cells (left panels). Relative GFP-diffusion-normalized quantification corresponding to fold-enrichment of RNA-binding proteins in SICs in ten different cells collected from three different experiments. Error bars represent±s.d.; ***$P \leq 0.001$, *$P \leq 0.05$ (two-tailed t-test). (D) Representative localization of mCherry-tagged Sam68 RNA-binding mutant (I184N and G178D), NLS mutant (R436-442A) and signaling mutants (Y435-440-443F) in adhering MRC-5 cells. All scale bars:10 µm. Enlarged images of the boxed areas are shown magnified ×2.5.
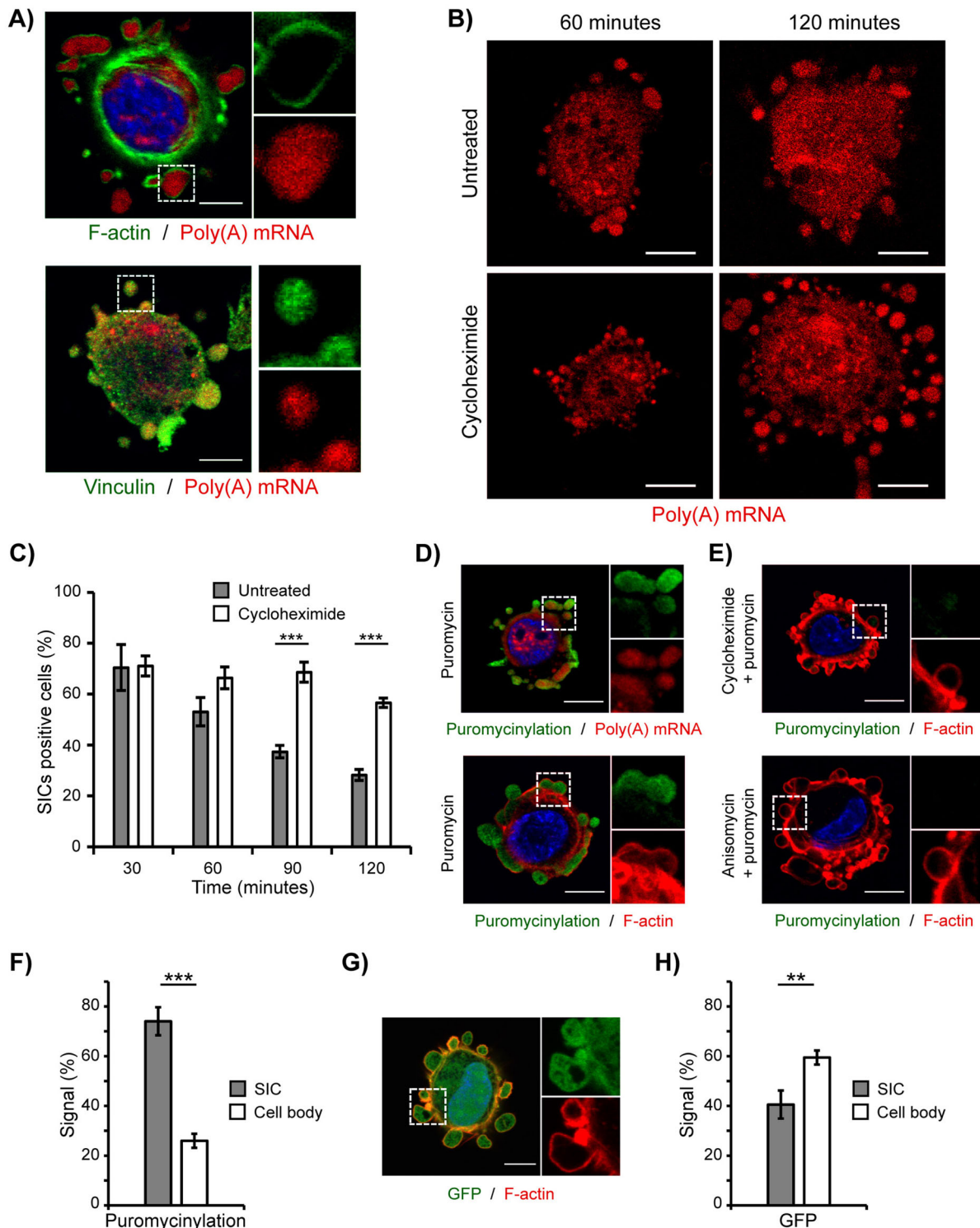
Fig. 3. Polyadenylated mRNA in spreading initiation centers (SICs). (A) Representative confocal mid-section plane of adhering MRC-5 cells hybridized with Alexa-Fluor-594-tagged oligo(dt) (red). Poly(A) mRNAs colocalized with two known components of SIC – F-actin and vinculin (green). (B) Representative image of MRC-5 cells in the presence or absence of 50 µg ml^{-1} of cycloheximide during the initial phase of adhesion. Poly(A) mRNAs were detected by using Alexa-Fluor-594-tagged oligo(dt) 25mers (red). (C) Statistical assessment of the number of SIC-positive cells over time with or without or cycloheximide treatment. Statistical analysis was performed on over 40 cells from triplicate adhesion assays for each condition. Error bars represent±s.d.; ***$P \leq 0.001$ (two-tailed t-test). (D) Representative image of puromycinylated proteins (green) and poly(A) mRNA by using Alexa-Fluor-594-tagged oligo(dt) (upper panel) or F-actin CF™568 phalloidin (lower panel), showing localized active translation within SICs in newly adhering cells. (E) Inhibition of puromycin incorporation in response to 50 µg ml^{-1} cycloheximide (upper panel) or 10 µg ml^{-1} anisomysin (lower panel) pretreament 15 min before the addition of puromycin. (F) Whole-cell assessment of the cellular distribution of puromycinylated proteins in adhering MRC-5. Error bars represent ±s.d.; ***$P \leq 0.001$ (two-tailed t-test). (G) Representative image of GFP distribution during the initial phase of cellular adhesion. F-actin was detected with CF™568 phalloidin (red). (H) Whole-cell assessment of the cellular distribution of GFP in adhering MRC-5 cells. Error bars represent±s.d.; **$P \leq 0.01$ (two-tailed t-test). All scale bars: 10 µm.

spreading. By contrast, this effect was not observed in HeLa cells, cells in which SICs are not present at the adhesion phase (Movie 3A and B).

To validate our observation, we quantified the cell adhesion kinetics of two SIC-positive cell lines (MRC-5 and NHDF) and two SIC-negative cell lines (HeLa and Caco-2) in presence or absence of cycloheximide. We found that cycloheximide treatment affected adhesion efficiency after 120 min in both MRC-5 and NHDF cells ($37\pm2\%$ and $38\pm4\%$ decrease, respectively), whereas no variation of adhesion dynamic was observed in HeLa and Caco-2 cells (Fig. 4A). This effect was not exclusive to cycloheximide because treatment with puromycin during the adhesion assay also decreased adhesion capacities of MRC-5 cells, while not affecting HeLa cell adhesion kinetics (Fig. S3A). Although cycloheximide and puromycin affect different aspect of translational mechanisms, treatment with either drug has the same outcome because they both rapidly inhibit *de novo* protein synthesis. Because some of the SIC-bound mRNA-binding proteins are known to restrain mRNA translation (Aulas et al., 2015; Klein et al., 2013; Mazroui et al., 2002), we reasoned that abrogating their expression should have an effect opposite to the one observed with translation inhibitors. As expected, knockdown of Sam68 and G3BP1 by using short hairpin RNA (shRNA) showed a slight increased adhesion kinetics, and a faster rate of SIC metabolism (Fig. S3B-D).

Interestingly, cell lines affected by cycloheximide also share a mesenchymal-like morphology, whereas cancer cell lines are epithelial-like. This was confirmed by the protein expression of specific epithelial and mesenchymal cell markers (Fig. 4B). These results suggest that the translation inhibition effect on adhesion is a mechanism shared by other mesenchymal cell lines, but not epithelial-like cells.

3D reconstitution of adhering MRC-5 cells showed a close relation between the actin cytoskeleton and SICs, pointing out their involvement in the maturation of focal adhesion and the establishment of cellular morphology (Fig. S4A). Actin architecture was completely absent in cycloheximide-treated adhering MRC-5 cells (Fig. S4B), which rather displayed an overt amoeboid morphology, a morphological adaptation of mesenchymal cells (Parri et al., 2009; Sahai and Marshall, 2003).

Interestingly, cancer cells that proceeded though EMT can also adopt an amoeboid-like morphology by undergoing MAT, suggesting that adhesion of these cancer cells is affected in a way similar to that of MRC-5 and NHDF cells.

Regulation of SICs and the amoeboid morphology

The transition between SIC-dependent adhesion and the subsequent spreading phase shares similarities with AMT. The only known discrepancy between both states is the level of activation of RhoA, a small GTPase involved in actin cytoskeleton remodeling, which is elevated in amoeboid cells and restrained in mesenchymal cell lines (Pinner and Sahai, 2008; Yamazaki et al., 2005).

Therefore, we evaluated the level of RhoA activation in SICs by using a purified GST-ROCK[967-1085] fusion protein that selectively binds RhoA-GTP, the active form of RhoA (Berdeaux et al., 2004). As expected, most of the active RhoA-GTP was localized in SICs (Fig. 5A). Detection of associated GST-ROCK[967-1085] was abrogated in cells expressing shRNA directed against RhoA (Fig. 5B-C). Quantification of the distribution of active RhoA showed an almost exclusive SIC localization when compared to total active RhoA throughout the cell (Fig. 5D). In light of these results, we assessed the effect of inactivation of the RhoA pathway has on adhesion of MRC-5 cell. Cells treated with the ROCK
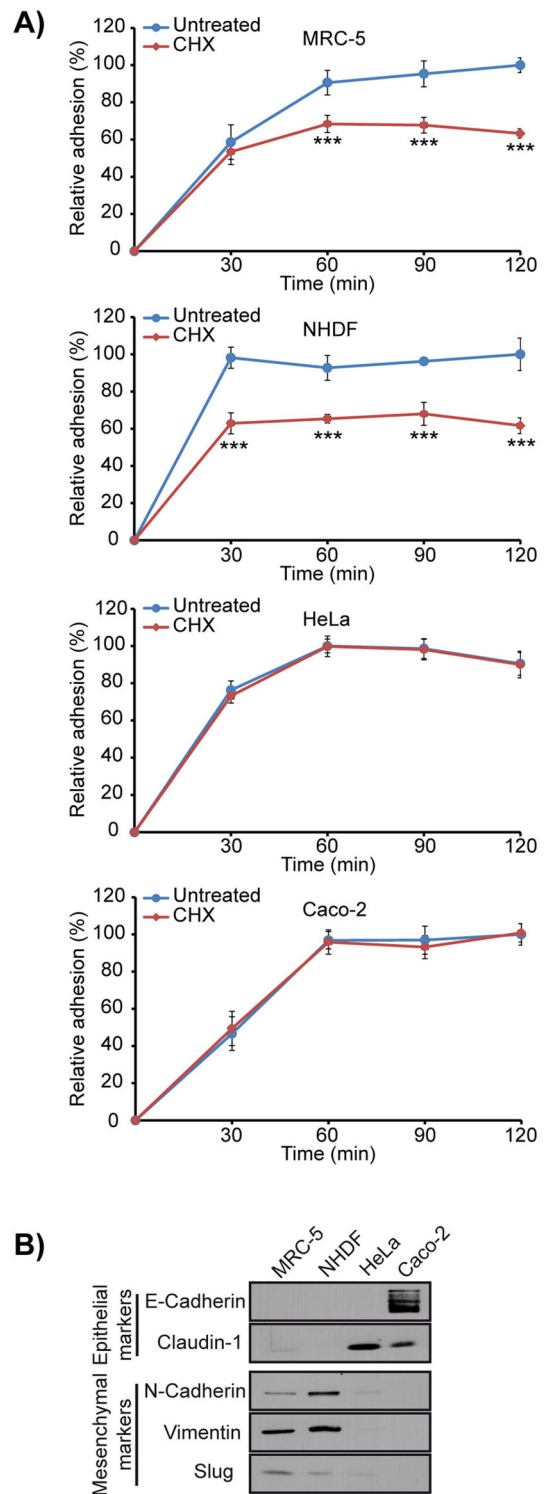
Fig. 4. Localized poly(A) mRNA translation within SICs during the initial phase of cellular adhesion. (A) Quantification of adhesion assays using MRC-5, NHDF, HeLa and Caco-2 cells in presence or absence of cycloheximide (50 µg ml^{-1}). ***$P\leq0.001$ (two-tailed t-test). (B) Western blotting of EMT markers (E-cadherin, claudin-1, N-cadherin, vimentin or Slug) on MRC-5, NHDF, HeLa and Caco-2 cells.

inhibitor Y27632 showed increased adhesion in the initial phase (Fig. 5E) with an increased spreading rate that bypassed SIC formation (Movie 4). This accelerated spreading seemed to have weakened the adhesion process because Y27632-treated cells lost
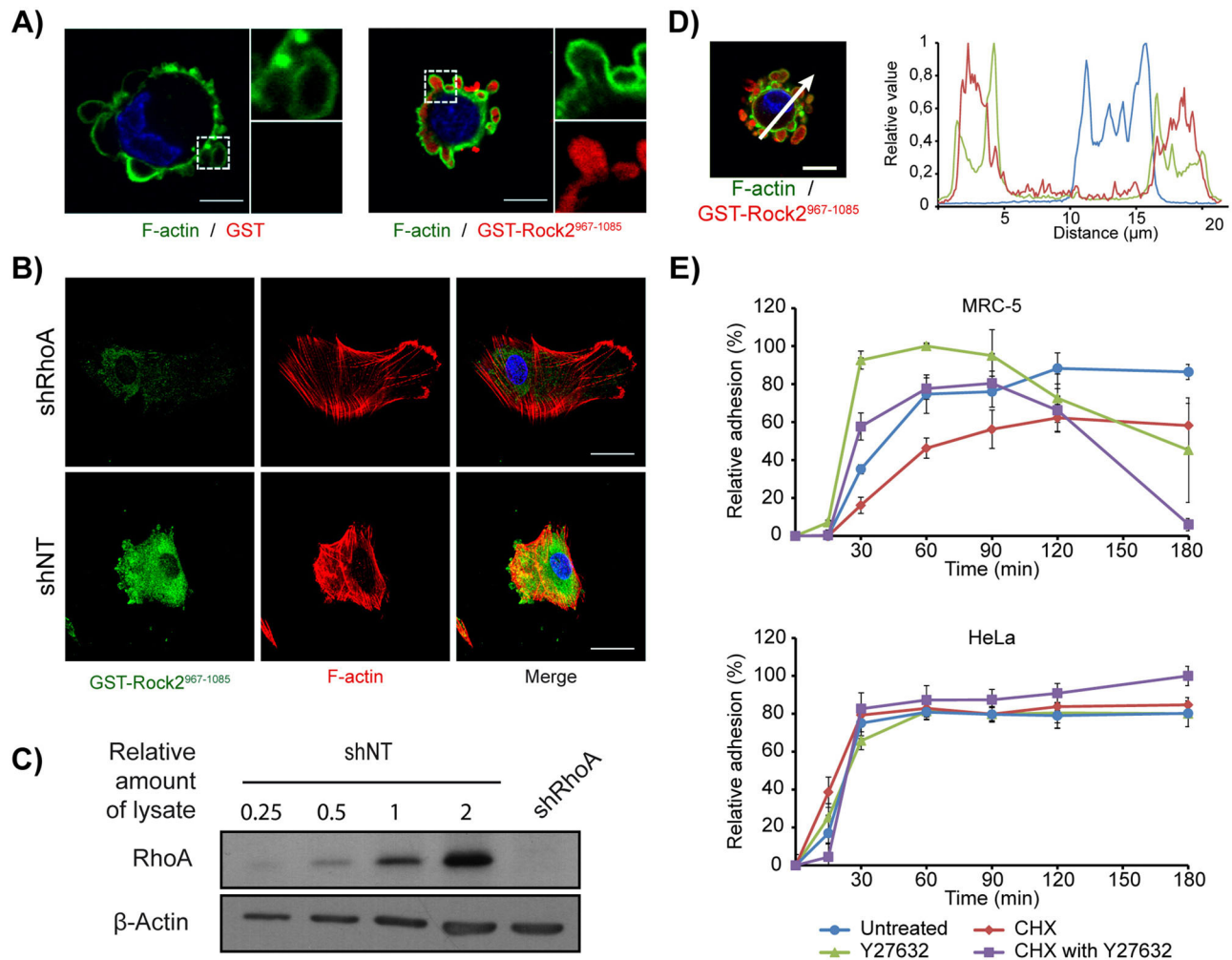
Fig. 5. SIC-dependent adhesion is affected by mRNA translation and GTPase activation. (A) Representative cellular distribution of the active forms of RhoA (RhoA-GTP) in newly adhering MRC-5 using purified recombinant GST-Rock2$^{967-1085}$ as a probe (right panel). The association of Rock2$^{967-1085}$ with RhoA-GTP was detected using an anti-GST antibody followed by a tertiary antibody coupled to Alexa Fluor 555 (red). GST was also used as a primary probe (negative control; left panel), validating that the observed signal was conferred by Rock2$^{967-1085}$ binding to its target and not GST. F-actin was detected using CFTM488 phalloidin (green). Enlarged images of the boxed areas are shown on the right magnified ×2.5. (B) Representative cellular distribution of active RhoA (with purified GST-Rock2$^{967-1085}$; green) or F-actin (with CF™568 phalloidin; red) in MRC-5 cells expressing RhoA shRNA (upper panel) or a non-target shRNA (lower panel). (C) Efficiency of RhoA shRNA in MRC-5 cells. RhoA protein expression in lysate of cells expressing non-targeting shRNA (shNT) or shRhoA. (D) Graphical representation of the amount of active RhoA in SICs. The graph represents the signal intensity of purified GST-Rock2 (red), which detects the active form of RhoA, F-actin (green) and DAPI (blue). Measurement was performed along the cell axis (indicated by the red arrow) of a representative adhering MRC-5 cell (left panel). (E) Quantification of adhesion assays on MRC-5 and HeLa cells treated with 50 μg ml^{-1} cycloheximide, 10 μM Rock inhibitor (Y27632) or both. Error bars represent±s.d.; all scale bars: 10 μm.

adherence with time. This effect was further increased when cycloheximide was combined with Y27632 treatment (Fig. 5E). Again, no effect was observed in HeLa cells, even when cells were treated with both cycloheximide and Y27632 (Fig. 5E). Similar results were obtained using MRC-5 expressing a shRNA directed against RhoA (Fig. S3E). Moreover, both Y27632 and shRhoA treatment provoked a faster rate of SIC metabolism compared to non-targeting shRNA (shNT)-expressing MRC-5 cells (Fig. S3F).

These results suggest that inactivation of the RhoA pathway interferes with the SIC-regulated adhesion process by forcing premature cellular spreading. This leaves the cells with a limited number of available adhesion complexes due to its inability to produce the necessary adhesion material needed for correct adhesion consolidation. This is supported by the observed combined effect of Y27632 and cycloheximide, a treatment that blocks all possible adhesion enhancements through *de novo* protein

synthesis. Overall, these results show that SIC-dependent adhesion relies on (i) localized translational events necessary for adhesion complex maturation and (ii) locally regulated activity of RhoA to limit spreading and consolidate adhesion. This does not seem to apply to epithelial cells, suggesting that their restrained spreading morphology allows them to remain adhered, even with limitited expression of adhesion components.

Adhesion-induced translational control depends on EMT

Adhered MRC-5 cells progressing to the subsequent spreading phase seemed to switch from an amoeboid to a mesenchymal-like morphology. The sequential change of morphology is similar to that observed in AMT. This could explain why epithelial-like cancer cells were not affected by treatments interfering with SIC metabolism because only mesenchymal-like cells can adopt an amoeboid morphology. It also suggest that only cancer cells that
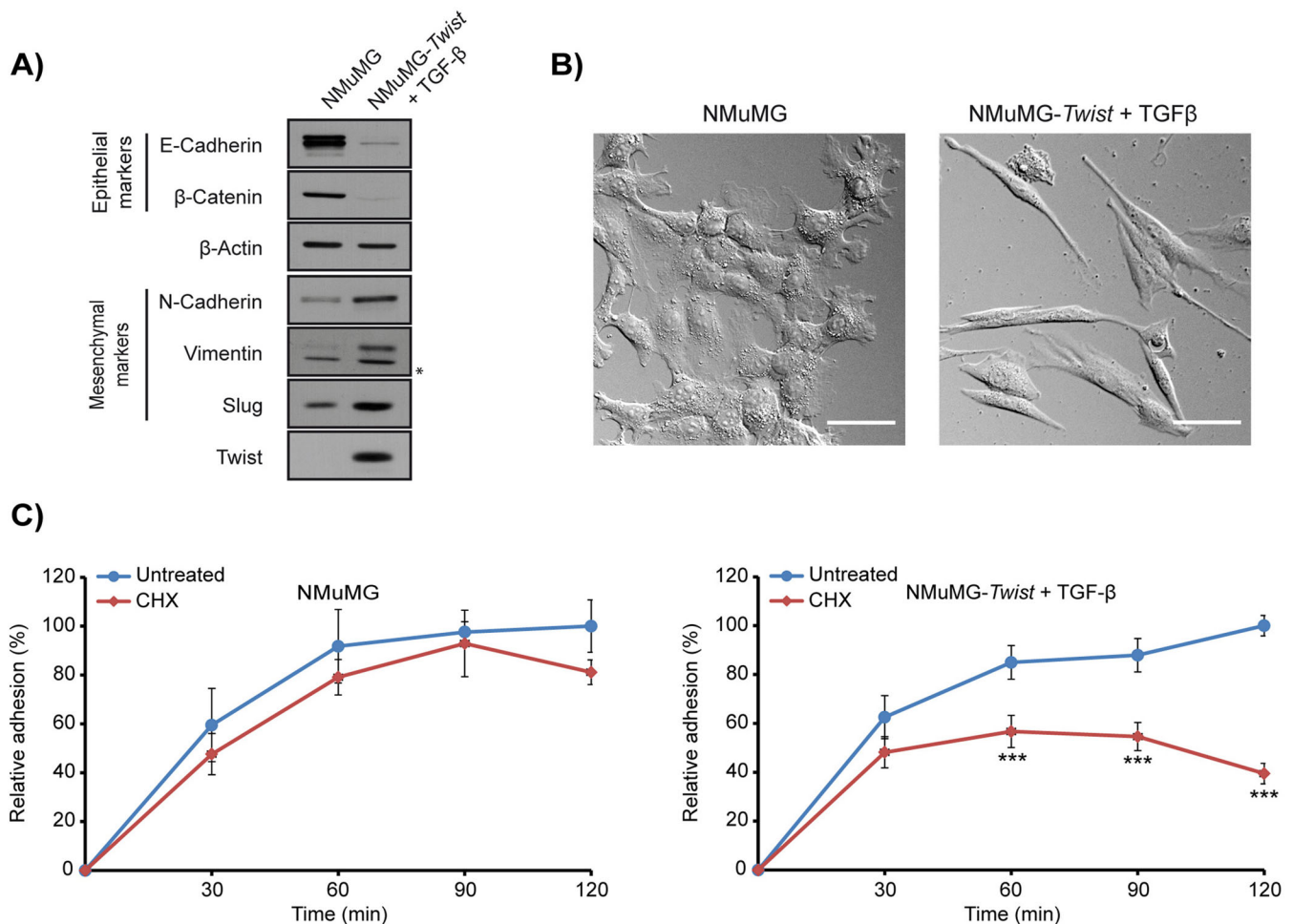
Fig. 6. Translation-induced adhesion regulation in EMT-inducible epithelial-like cells. (A) Detection of EMT markers (E-cadherin, β-catenin, β-actin, N-cadherin, vimentin, Slug or Twist) on untreated and EMT-induced NMuMG cells; *, unspecific band. (B) Representative images of NMuMG cells and their morphological transition following induction of EMT. Scale bars: 50 µm. (C) Quantification of adhesion assays using untreated and EMT-induced NMuMG cells in presence or absence of cycloheximide (50 µg ml^{-1}). Error bars represent±s.d.; ***$P \leq 0.001$ (two-tailed t-test).

proceed through EMT share mechanisms that are observed in SIC-positive cells. In order to determine whether the morphological state has an impact in SIC-dependent adhesion, we compared the adhesion kinetics of EMT-inducible NMuMG cells (Ngan et al., 2013; Northey et al., 2008). Transition of epithelial NMuMG cells towards mesenchymal-like cells was achieved by the transducing transcription factor Twist followed by sustained treatment with TGF-β (Miettinen et al., 1994; Yang et al., 2004). As expected, we observed a substantial decrease in the expression of epithelial cell markers, while detecting increased expression of mesenchymal markers following induction of EMT (Fig. 6A). Induction efficiency was corroborated by morphological changes associated with EMT (Fig. 6B). Adhesion assays using EMT-induced cells showed significantly longer adhesion latency in the presence of the protein synthesis inhibitor cycloheximide, whereas no effect was observed in a non-induced counterpart (Fig. 6C). The relevance of the morphological state in this translation-regulated adhesion process was further supported by another well-known inducible EMT model, the MDCK cells. Indeed, only EMT-induced MDCK gained adhesion-related sensibility to translational inhibitor (Fig. S3G), as observed with NMuMG cells.

To assess any possible changes in cycloheximide sensitivity conferred by the combined *Twist* expression and TGF-β treatment, we induce EMT using only exogenous *Twist* expression or TGF-β

treatment. As shown in Fig. S3H, either treatment induced similar adhesion-related sensitivity to translation inhibitors.

These results suggest that invasive cancer cell lines proceeding through EMT – such as TGF-β-induced NMuMG cells – use SIC-associated mechanisms to modulate their adherence, which allows them to migrate and invade peripheral tissue.

SIC metabolism as a model of metastatic cancer cell adhesion and transendothelial migration

Our data suggest that a mechanism regulating SIC metabolism is used to increase the invasion potential of metastatic cancer cells that undergo EMT. To assess this possibility, we compared the highly metastatic breast cancer cell line MDA-MB-231 to its less metastatic counterpart MDA-MB-468 (Brunner et al., 1993; Cailleau et al., 1978). The selection of those two cell lines was based on the expression levels of the different EMT markers. As seen in Fig. 7A, MDA-MB-231 cells clearly showed a mesenchymal profile whereas MDA-MB-468 cells showed an epithelial profile. We then performed an *in vitro* adhesion assay using these two cell lines. As expected, cycloheximide reduced MDA-MB-231 cell adhesion by >60% (67±6% decrease), whereas no significant effect was observed with MDA-MB-468 cells under the same conditions (Fig. 7B).

To determine whether translation inhibitors also impairs cancer cell adhesion to the blood vessel wall, we performed an adapted
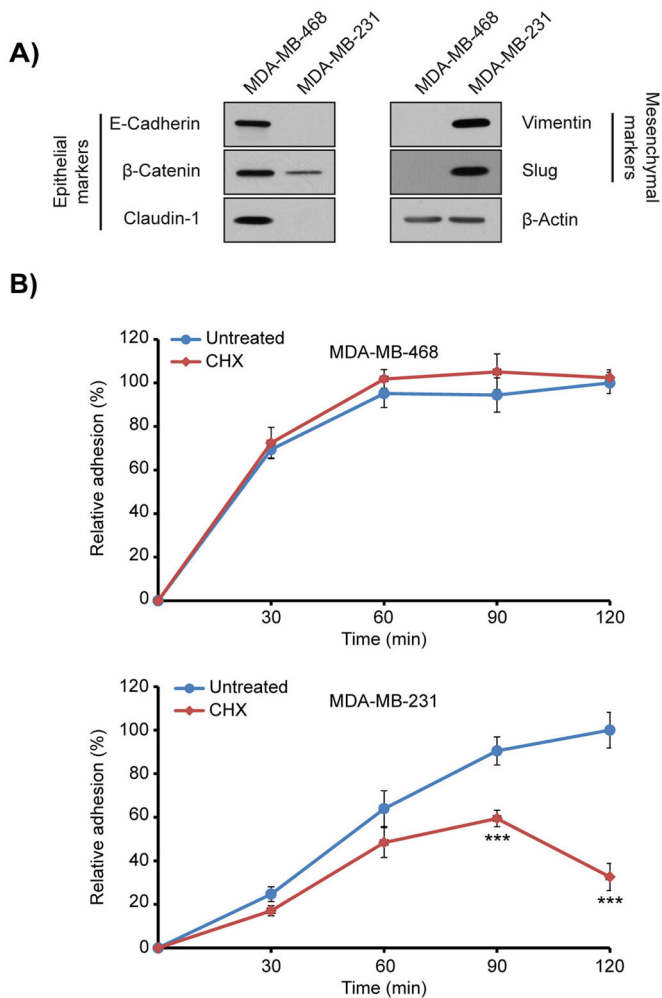
Fig. 7. Translation-induced adhesion regulation in invasive and non-invasive cancer cell lines. (A) Detection of EMT markers on breast cancer cells of low (MDA-MB-468) and high (MDA-MB-231) metastatic capacity. (B) Quantification of adhesion assays using MDA-MB-468 and MDA-MB-231 cells, in presence or absence of cycloheximide (50 µg ml^{-1}). Error bars represent±s.d.; ***$P \leq 0.001$ (two-tailed t-test).

adhesion assay using human umbilical vein endothelial cells (HUVECs) (Gout et al., 2006). By integrating a puromycin resistance gene in HUVECs, we were able to assess the effect of puromycin on MDA cell adhesion to the endothelial cell layer without affecting its integrity. As shown in Fig. 8A, adhesion of MDA-MB-231 cells to the endothelial layer was also reduced by >60% in presence of puromycin, whereas no significant effect was observed for MDA-MB-468 cells (Fig. 8B). We reasoned that the effect on adhesion should have a major impact on the invasion capacity of MDA-MB-231 cells. To quantify this effect, we performed a Boyden chamber invasion assay by using puromycin-resistant HUVECs. Again, the invasion capacity of MDA-MB-231 cells was affected by puromycin treatment. Indeed, <30% of the seeded MDA-MB-231 cells were able to invade the HUVEC monolayer (Fig. 8C). These results indicate that – in cancer cells that have transited through a mesenchymal-like morphology – impairment of SIC-associated adhesion mechanisms drastically decreases their adhesion potential, as well as their ability to invade through sheets of endothelial cells, the main component of blood and lymph vessel.

DISCUSSION

Our study shows that specific RNA-binding proteins known for their ability to regulate mRNA processes – such as Sam68, G3BP1 and FMRP – are enriched in early adhesion structures termed SICs. We also found that SICs also contain polyadenylated mRNAs and that their localized translation is involved in the initial phase of adhesion consolidation in seeding primary cells. We show that this new adhesion mechanism is shared by cells that present a mesenchymal-like profile, whereas epithelial-like cells are completely unaffected. Hence, we propose that RNA-binding-mediated localized translation can modulate early adhesion of mesenchymal-like cells – such as metastatic cells – that proceeded through EMT.

Although SICs have been shown to be involved in cellular spreading, their contribution to early adhesion processes remain ill defined. In a large-scale SILAC analysis, SICs have been found to potentially contain focal adhesion markers, ribosomal RNA and a surprisingly high number of RNA-binding proteins (de Hoog et al., 2004). We found that the RNA-binding protein Sam68 and its mRNP-associated proteins G3BP1 and FMRP, are enriched within SICs, and mutation of the RNA-binding domain abrogates cytoplasmic relocalization of Sam68 during early adhesion. This suggests that RNA association is an essential process for Sam68 localization in SICs and that this mechanism is shared by other RNA-binding proteins that were identified as SIC components.

Our Alexa-Fluor-596-tagged oligo(dT) probe showed clearly positive in SICs, demonstrating the presence of poly(A) mRNA colocalizing with other SIC components, such as focal adhesion proteins and RNA-binding proteins. Neuronal Sam68 and FMRP have both been shown to be part of complexes that transport translationally repressed RNPs in order to growth cones for localized translation (Christie et al., 2009; Klein et al., 2013; Zhang et al., 2015). Similarly, repressed RNPs might be translocated to SICs for rapid and localized translation upon adhesion-activating signals. This was further supported by a puromycin incorporation assay showing that >70% of neosynthesized puromycinylated proteins are localized to SICs, which indicates that a large portion of translational activity is confined within these structures during early adhesion. Thus, the effects that – upon addition of translation inhibitors – were observed on cell adhesion are probably caused by misexpression of these SIC-associated mRNAs, although we cannot exclude the possibility that inhibition of translation of some mRNA that is usually translated outside of these structures, might also contribute to some of those effects.

Our results show that localized translation is directly linked to SIC turnover. Indeed, translation inhibition provoked SIC accumulation in adhering cells and also altered cell adhesion kinetics. One way to explain this effect is that cells need rapid translation of structural and signaling proteins involved in cell adhesion and focal adhesion site formation. Sustained inhibition of translation decreased localized production of these molecules, weakening early adhesion complex integrity and impairing their ensuing maturation in focal adhesion sites. It is also possible that neosynthesized proteins are involved in membrane remodeling inhibition induced by RhoA activation in SICs. Our results indicate that both of these processes take place in adhering cells because treatment with a ROCK inhibitor (Y27632) repressed SIC formation while provoking uncontrolled spreading and weakened adhesion. This effect was more obvious during translation inhibition, suggesting that locally translated adhesion molecules contribute to adhesion consolidation and maturation of the focal adhesion site. Although this result does not show a clear epistatic relationship
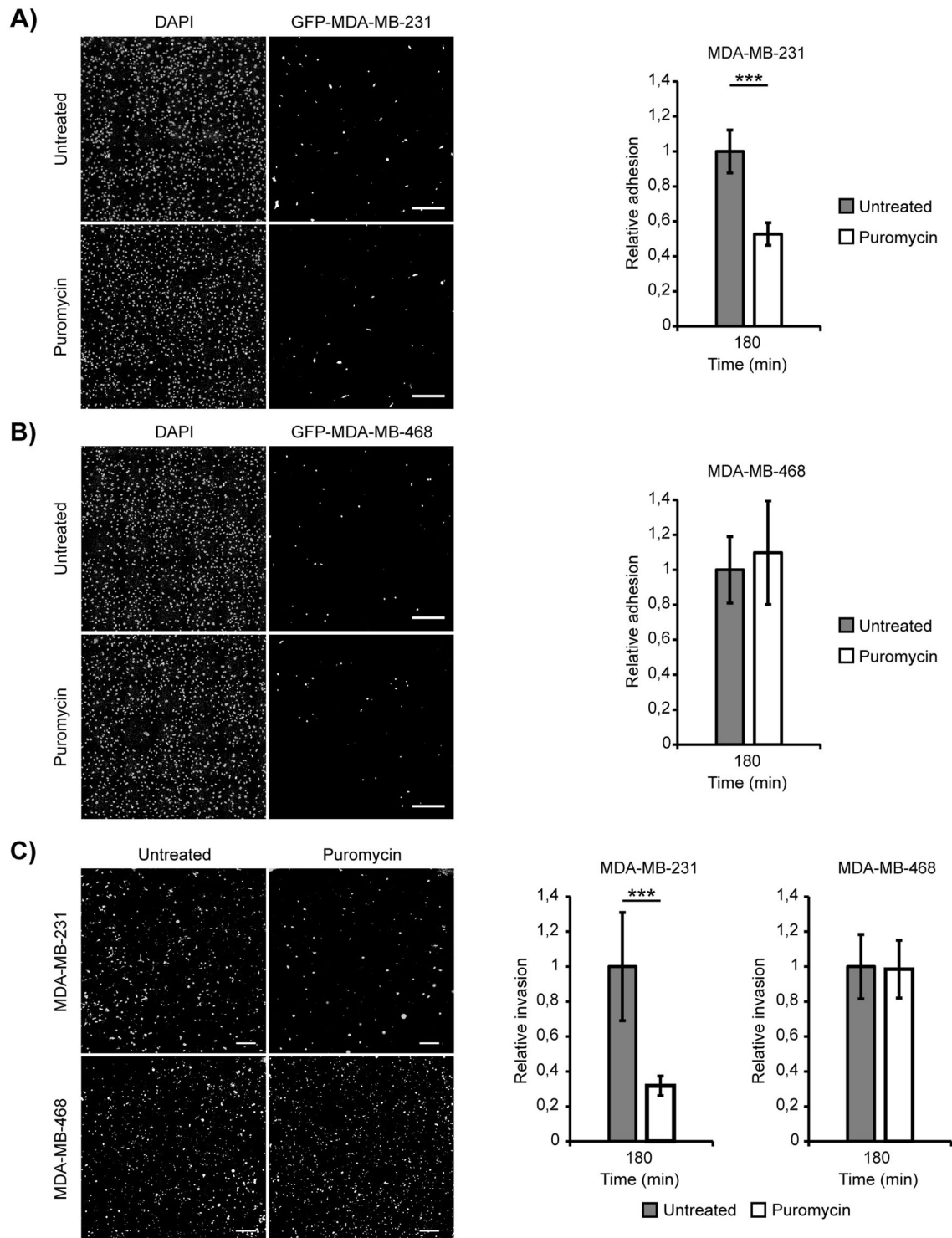
Fig. 8. Translational inhibition in metastatic cancer cell impairs adhesion and transendothelial invasion. (A) Representative image corresponding to 64 stitched 20× acquisitions of MDA-MB-231 cells adhering on a puromycin-resistant HUVEC monolayer, in presence or absence of puromycin (2.5 µg ml^{-1}). Scale bars: 300 µm. (B) Representative image corresponding to 64 stitched 20× acquisitions of MDA-MB-468 cells adhering on a puromycin-resistant HUVEC monolayer, in presence or absence of puromycin (2.5 µg ml^{-1}). Scale bars: 300 µm. (C) Representative image corresponding to 64 stitched 20× acquisitions of MDA-MB-231 and MDA-MB-468 cells that show transendothelial invasion through a puromycin-resistant HUVEC monolayer. The assays were done in presence or absence of puromycin (2.5 µg ml^{-1}). Scale bars: 500 µm. Error bars represent±s.d.; ***$P \leq 0.001$ (two-tailed t-test).

between treatment with cycloheximide or Y27632, it strongly suggests the necessity of a tight regulation of SIC-localized mRNA translation and cytoskeletal rearrangement for correct adhesion of MRC-5 cells and, potentially, other mesenchymal cells.

On the one hand, it has been suggested previously that SICs are only found in non-transformed primary cell lines (de Hoog et al., 2004) and only cell lines producing SICs showed impaired adhesion kinetics upon treatment with a translation inhibitor.

Cancer cell lines, such as HeLa and CaCo-2 cells, do not produce SICs during the adhesion process and their adhesion kinetics are not affected by translation inhibition. Our results support the idea that cancer cell lines bypass SIC formation and directly proceed to the spreading phase without relying on SIC-induced translation events. On the other hand, both cell lines affected by translation inhibition (MRC-5 and NHDF) also share a mesenchymal-like morphology, whereas both cancer cell lines (HeLa and CaCo-2) are more epithelial-like. This was confirmed by the expression pattern of specific epithelial and mesenchymal markers. Moreover, adhering SIC-positive cells share common morphological features with amoeboid cells (i.e. low adhesion, peripheral blebbing and increased RhoA activity) (Sanz-Moreno et al., 2008; Wilkinson et al., 2005). When these amoeboid-like SIC-positive adhering cells initiate the subsequent spreading phase, they switched to a mesenchymal-like morphology, with increased adherence and limited RhoA activity. This sequential change in morphology is similar to that observed in AMT, which supports the idea that epithelial-like cancer cells are not affected by treatments that interfere with SIC metabolism because only mesenchymal-like cells can adopt an amoeboid morphology.

This latter idea is further supported in studies that have used the well-established NMuMG and MDCK cell lines to induce EMT (Ngan et al., 2013; Yang et al., 2004); in both cell lines induction of EMT was only affected by a translation inhibitor upon mesenchymal induction. Although we failed to detect SICs in these cells, we recapitulate mechanisms that can usually be found during adhesion initiation in these structures. As most cancer cell lines are derived from simple epithelium, it is fair to assume that not all cancer cell adhesion is regulated through translational mechanisms, such as that observed in SICs. This also suggests that the restrained spreading morphology of cancer cells allows them to remain adhered, even when the expression of adhesion components is limited in response to inhibition of translation. Still, our results obtained with NMuMG cells led us to postulate that mechanisms that regulate SIC metabolism are involved in the invasion potentiation of cancer cells that proceed through EMT.

To assess this possibility, we screened MDA-MB breast cancer cell lines and selected those that showed the strongest discrepancy between epithelial and mesenchymal marker profiles. MDA-MB-231 cells presented a clear mesenchymal profile, whereas MDA-MB-468 only expressed epithelial markers. Again, these cell lines followed similar patterns because only the adhesion potential of MDA-MB-231 cells was affected under translation repression. This was also observed in *in vitro* and HUVEC adhesion assays. This effect was not restricted to adhesion because inhibition of translation also affected transendothelial migration of MDA-MB-231 cells. Indeed, by using standard Boyden chambers coated with HUVECs, we expected a cellular behavior similar to that seen in adhesion assays. However, we found that the effect was even greater for transendothelial migration. Indeed, the proportion of cells that migrated through HUVEC monolayers was even lower than of cells that adhered to the monolayer. This might be because of the inability of adhering cells to transit from an amoeboid-like to a mesenchymal-like morphology during translation inhibition at early adhesion. Low adhesion potentials conferred by the amoeboid morphology is most probably not strong enough to allow newly adhering cells to migrate through the endothelial monolayer. Although restricted to a limited number of cell lines, our result suggests that the described translation-regulated adhesion also occurs in other metastatic cancer cells. Further studies will be required to assess whether this mode of regulation can be observed in other highly metastatic cells that transit to a mesenchymal-like morphological state.

In summary, our current study defines how the regulation of localized mRNA translation can affect metastatic cell adhesion to the endothelium and impacts on their invasion capacity. Although SIC formation might not be required for this process, the molecular mechanism that takes place within these structures is essential for metastatic cells that successfully progress through EMT. Hence, SICs offer a secluded structure that might help us to define the molecular switch and to identify specific mRNA targets regulating this so-far-unknown adhesion checkpoint. This, in turn, might allow the development of new strategies to inhibit metastatic cell adhesion and invasion in later stages of cancer progression, such as metastasis.

MATERIALS AND METHODS
Cell culture
Human embryonic lung fibroblast (MRC-5), human colorectal adenocarcinoma (CaCo-2), HeLa and HEK 293T cells were cultured in Dulbecco's modified Eagle's (DMEM) medium (219-010; Wisent) supplemented with 10% fetal bovine serum (FBS; Gibco). Normal human dermal fibroblasts (NHDF) were cultured in FBM (CC3131; Lonza). Mouse mammary gland epithelial (NMuMG) cells were cultured in DMEM supplemented with 10% FBS, 2 mM L-glutamine (Wisent), 10 mM HEPES pH 7.4 and 10 μg ml^{-1} insulin. Human umbilical vascular endothelium cell (HUVEC) cultures were maintained in endothelial cell growth medium 2 (EGM2; CC3156; Lonza). Replicated cultures were obtained by trypsination and were passaged up to six times. Human breast cancer cells (MDA-MB)-231 (high metastatic capacity) or MDA-MB-468 (low metastatic capacity) were cultured in Leibovitz's L-15 medium (41300-039; Gibco) supplemented with 10% FBS and maintained at 37°C without CO_2 supplementation. All cell lines used in this manuscript were purchased from ATCC and experiments were performed by using cells from the original ATCC vial.

Viral infection
Lentiviral particles were generated by transfecting HEK 293T cells with 12 μg of pLJM1 vector (Addgene plasmid #19319), 6 μg of psPAX2 packaging plasmid (Addgene plasmid #12260) and 2 μg pMD2.G envelope plasmid (Addgene plasmid #12259). Medium was changed 16 h after transfection and lentiviral particles were harvested 24 h later. Viral supernatant was filtered through 0.45 μm filters and supplemented with 8 μg ml^{-1} polybrene (Sigma). Supernatant was added to the cells for 6 h before DMEM was added for overnight incubation. *Twist* cDNA from pBabe-puro-mTwist (Addgene plasmid #1783) was cloned into pLJM1.

Immunofluorescence and *in situ* hybridization
Cells were fixed with 4% paraformaldehyde in 1× phosphate-buffered saline (PBS) for 20 min at room temperature (RT) and permeabilized with 1% Triton X-100 in PBS for 5 min at RT. Immunostaining was obtained using the following antibodies: anti-vinculin diluted at 1:200 (4505; BD Bioscience), anti-Sam68 diluted at 1:200 (Chen et al., 1999), anti-G3BP1 diluted at 1:1000 (Gallouzi et al., 1998), anti-FMRP diluted at 1:1 (Fournier et al., 2013), anti-paxillin diluted at 1:100 (610052; BD Bioscience), pAb anti-GST diluted at 1:100 (2625; Cell Signaling), anti-puromycin diluted at 1:10,000 (12D10; Millipore), Alexa Fluor 488 goat anti-rabbit IgG (4412; Cell Signaling) and Alexa Fluor 555 goat anti-rabbit IgG (4413; Cell Signaling). Polymerized actin was visualized by using CF™568 phalloidin (00044; Biotium) or CF™488 phalloidin (00042; Biotium). Polyadenylated mRNAs were detected by using a custom-made 5′-tagged Alexa Fluor 594 oligo(dt) (25mer) probe from Invitrogen. Active RhoA (RhoA-GTP) visualization was performed using purified recombinant GST-Rock2$^{967-1085}$ as the primary probe. GST-Rock2$^{967-1085}$ that was associated with RhoA-GTP was detected using the aforementioned anti-GST followed by the Alexa-Fluor-555-conjugated goat anti-rabbit IgG. Cells were fixed in 4% paraformaldehyde solution, washed three times with 1× PBS and permeabilized in PBS supplemented with 0.2% Triton×100 (15 min at RT). Coverslips were hybridized for 15 min at 42°C in hybridization solution (2×SSC, 1 mg/ml

t-RNA, 10% dextran sulfate (w/v) and 25% formamide). Cells were then incubated for 16 h at 37°C in hybridization solution supplemented with 2 µg ml^{-1} Alexa-Fluor-594-tagged oligo(dt) probe. Cells were washed twice with 2×SSC at 42°C followed by two washes with 0.5× SSC at 42°C and finally fixed a second time in 4% paraformaldehyde (15 min at RT) for immunofluorescence staining. DNA was stained with 4′,6′-diamidino-2-phenylindole (DAPI). Immunofluorescent images were obtained by using a 60× lens (1.42 NA, splan APO) mounted on an FV1000 confocal laser-scanning microscope driven by FluoView software. Image acquisition was performed at RT and images were processed using FluoView software (Olympus). Brightness–contrast adjustment and panel montage were made using Illustrator CS6 (Adobe). All inserts in figures correspond to a 2.5× magnification of the selected area.

RNA interference
Sam68 shRNA (5′-CCGGGAGCAAAGTTGTTACTGATTTCTTGCTC-GAGCAAGAAATCAGTAACAACTTTGCTCATTTTTTG-3′ and 5′-AA-TTCAAAAAATGAGCAAAGTTGTTACTGATTTCTTGCTCGAGCAA-GAAATCAGTAACAACTTTGCTC-3′), G3BP1 shRNA (5′-CCGG<u>ACA-TTTAGAGGAGCCTGTTGCTGAAC</u>TCGAGTTCAGCAACAGGCTC-CTCTAAATGTTTTTTG-3′ and 5′-AATTCAAAAAACATTTAGAGG-AGCCTGTTGCTGAACTCGAGTTCAGCAACAGGCTCCTCTAAAT-GT-3′), RhoA shRNA (5′-CCGG<u>TGGAAAGACATGCTTGCTCATC</u>-TCGAGATGAGCAAGCATGTCTTTCCATTTTTG-3′ and 5′-AATTC-AAAAATGGAAAGACATGCTTGCTCATCTCGAGATGAGCAAGCA-TGTCTTTCCA-3′) and control shRNA (5′-CCGGG<u>CGCGATAGCGCT-AATAATTT</u>CTCGAGAAATTATTAGCGCTATCGCGCTTTTTG-3′ and 5′-AATTCAAAAAGCGCGATAGCGCTAATAATTTCTCGAGAAATT-ATTAGCGCTATCGCGC-3′) were generated by ligation of oligonucleo-tids into the *Age*I and *Eco*RI restriction sites of pLKO.1 (Addgene plasmid #8453). Underlined sequences represent the targeted sequences.

Protein detection
Immunoblotting was performed by using the polyclonal antibodies (pAbs) anti-Sam68 AD1 (Chen et al., 1999), anti-vimentin (550513; BD Bioscience), anti-β-actin (8457; Cell Signaling), anti-N-cadherin (610920; BD Bioscience), anti-E-cadherin (610181; BD Bioscience), anti-claudin (13255; Cell Signaling), anti-β-catenin (13255; Cell Signaling), anti-Twist (sc-81417; Santa Cruz) and anti-Slug (9585; Cell Signaling). Immunoreactive proteins were visualized by using either goat anti-mouse (7076; Cell Signaling) or goat anti-rabbit (7074; Cell Signaling) antibodies conjugated to horseradish peroxidase, and the chemiluminescence (ECL) detection kit (NEL104001EA; Perkin-Elmer).

In vivo translation analysis
5 µg ml^{-1} of puromycin (PJ593; Bio Basic) was added during the last 5 min of a 60 min adhesion assay (using µ-Dish $^{35\ mm,\ high}$, cat. no. 81156, Ibidi). Puromycin incorporation within the elongating polypeptide was assessed by using anti-puromycin 12D10 (MABE343; Millipore) and visualized according to the SUnSET method (Schmidt et al., 2009). Cellular distribution of puromycin incorporation was verified by using ImageJ software on Z-stacks images covering whole-cell signals on more than ten cells from triplicate adhesion assays for each condition. Puromycin signals were quantified using unprocessed images; image acquisition was carried out under identical imaging conditions, without saturated pixels, using the FluoView software. Error bars for quantification are ±s.d.

In vitro adhesion assay
Exponentially growing cells were detached using 0.025% trypsin with 0.1% EDTA. Cells were counted and treated (according to treatment description in figure legends) before being plated on a 96-well Stripwell (Corning), and incubated at 37ºC, 5% CO$_2$ for 30-min intervals (e.g. 0, 30, 60, 90, 120 min). Seven replicates were done for each time point. Thereafter, cells were fixed with 4% paraformaldehyde for 20 min and nuclei were stained with DAPI (1 µg ml^{-1}). Fluorescence intensity was measured (excitation 355 nm, emission 460 nm) using a Fluoroskan Ascent Microplate Fluorometer (Thermo Scientific). Empty wells were used as a control to subtract background. Error bars for quantification are ±s.d.

Live-cell adhesion assay
Puromycin-resistant endothelial cells were obtained by lentiviral transduction of the puromycin resistance gene. 2×10^5 HUVECs were plated on gelatinized 35-mm glass Petri dishes (Word Precision Instruments) and grown to confluency in EGM2 supplemented with puromycin (0.5 µg ml^{-1}) for 48–72 h. Exponentially growing MDA-MB-231 and MDA-MB-468 cells in suspension that had been infected with lentivirus carrying GFP were trypsinized and treated with puromycin or vehicle for 30 min. EGM2 was exchanged for EGM2 containing puromycin or vehicle only and treated MDA cells were incubated to adhere onto endothelial cell layers. Three hours later, cells were washed gently with PBS, fixed and processed for DAPI staining. Images (64 per Petri dish) were captured at 20× magnification by using a Nikon Eclipse Ti fluorescence microscope with the 'Large Image function' driven by the NIS-Element software. Every condition was analysed in triplicate and statistics were carried out on four 8×8 20× field for each replicate. Error bars for quantification are ±s.d.

Cell migration and invasion assays
25,000 puromycin-resistant endothelial cells (HUVEC) were plated on gelatinized membranes (pore size 50 µm) of modified Boyden chambers (6.5 mm; Corning Transwell) and grown to confluency in EGM2 (48–72 h); simultaneously cells were plated onto a 35 mm Petri dish and grown to the same density to monitor confluency. Exponentially growing MDA-MB-231 and MDA-MB-468 cells were trypsinized and treated in suspension with puromycin or vehicle for 30 min. EGM2 in the upper part of the Boyden chamber was exchanged for EGM2 supplemented with puromycin or vehicle only, and MDA cells were transferred into the upper part of the Boyden chamber. Three hours later, cells on the upper part of the membrane were washed and scraped, whereas those that had migrated to the lower part were imaged at 20× magnification. Representative images correspond to 8×8 acquisitions stitched together by using the 'Large Image function' driven by the NIS-Element software to form a composite image of 64 fields at 20× magnification for each Transwell insert. Every condition was analysed in triplicate. Error bars for quantification are ±s.d.

Supplementary information
Supplementary information available online at
http://jcs.biologists.org/lookup/doi/10.1242/jcs.191320.supplemental

References
Andersson, M. K., Ståhlberg, A., Arvidsson, Y., Olofsson, A., Semb, H., Stenman, G., Nilsson, O. and Åman, P. (2008). The multifunctional FUS, EWS and TAF15 proto-oncoproteins show cell type-specific expression patterns and involvement in cell spreading and stress response. *BMC Cell Biol.* **9**, 37.
Aulas, A., Caron, G., Gkogkas, C. G., Mohamed, N.-V., Destroismaisons, L., Sonenberg, N., Leclerc, N., Parker, J. A. and Vande Velde, C. (2015). G3BP1

promotes stress-induced RNA granule interactions to preserve polyadenylated mRNA. *J. Cell Biol.* **209**, 73-84.

Bennett, L. L., Jr, Ward, V. L. and Brockman, R. W. (1965). Inhibition of protein synthesis in vitro by cycloheximide and related glutarimide antibiotics. *Biochim. Biophys. Acta* **103**, 478-485.

Berdeaux, R. L., Díaz, B., Kim, L. and Martin, G. S. (2004). Active Rho is localized to podosomes induced by oncogenic Src and is required for their assembly and function. *J. Cell Biol.* **166**, 317-323.

Brünner, N., Boysen, B., Rømer, J. and Spang-Thomsen, M. (1993). The nude mouse as an in vivo model for human breast cancer invasion and metastasis. *Breast Cancer Res. Treat.* **24**, 257-264.

Cailleau, R., Olivé, M. and Cruciger, Q. V. (1978). Long-term human breast carcinoma cell lines of metastatic origin: preliminary characterization. *In Vitro* **14**, 911-915.

Chen, T., Boisvert, F.-M., Bazett-Jones, D. P. and Richard, S. (1999). A role for the GSG domain in localizing Sam68 to novel nuclear structures in cancer cell lines. *Mol. Biol. Cell* **10**, 3015-3033.

Christie, S. B., Akins, M. R., Schwob, J. E. and Fallon, J. R. (2009). The FXG: a presynaptic fragile X granule expressed in a subset of developing brain circuits. *J. Neurosci.* **29**, 1514-1524.

David, A., Dolan, B. P., Hickman, H. D., Knowlton, J. J., Clavarino, G., Pierre, P., Bennink, J. R. and Yewdell, , J. W. (2012). Nuclear translation visualized by ribosome-bound nascent chain puromycilation. *J. Cell Biol.* **197**, 45-57.

de Hoog, C. L., Foster, L. J. and Mann, M. (2004). RNA and RNA binding proteins participate in early stages of cell spreading through spreading initiation centers. *Cell* **117**, 649-662.

Diz-Muñoz, A., Krieg, M., Bergert, M., Ibarlucea-Benitez, I., Muller, D. J., Paluch, E. and Heisenberg, C.-P. (2010). Control of directed cell migration in vivo by membrane-to-cortex attachment. *PLoS Biol.* **8**, e1000544.

Fallini, C., Donlin-Asp, P. G., Rouanet, J. P., Bassell, G. J. and Rossoll, W. (2016). Deficiency of the survival of motor neuron protein impairs mRNA localization and local translation in the growth cone of motor neurons. *J. Neurosci.* **36**, 3811-3820.

Fidler, I. J. (2003). The pathogenesis of cancer metastasis: the 'seed and soil' hypothesis revisited. *Nat. Rev. Cancer* **3**, 453-458.

Fournier, M.-J., Coudert, L., Mellaoui, S., Adjibade, P., Gareau, C., Cote, M.-F., Sonenberg, N., Gaudreault, R. C. and Mazroui, R. (2013). Inactivation of the mTORC1-eukaryotic translation initiation factor 4E pathway alters stress granule formation. *Mol. Cell. Biol.* **33**, 2285-2301.

Friedl, P., Borgmann, S. and Bröcker, E. B. (2001). Amoeboid leukocyte crawling through extracellular matrix: lessons from the Dictyostelium paradigm of cell movement. *J. Leukoc. Biol.* **70**, 491-509.

Gallouzi, I.-E., Parker, F., Chebli, K., Maurier, F., Labourier, E., Barlat, I., Capony, J.-P., Tocque, B. and Tazi, J. (1998). A novel phosphorylation-dependent RNase activity of GAP-SH3 binding protein: a potential link between signal transduction and RNA stability. *Mol. Cell. Biol.* **18**, 3956-3965.

Gout, S., Morin, C., Houle, F. and Huot, J. (2006). Death receptor-3, a new E-Selectin counter-receptor that confers migration and survival advantages to colon carcinoma cells by triggering p38 and ERK MAPK activation. *Cancer Res.* **66**, 9117-9124.

Griffin, B. A., Adams, S. R. and Tsien, R. Y. (1998). Specific covalent labeling of recombinant protein molecules inside live cells. *Science* **281**, 269-272.

Grünert, S., Jechlinger, M. and Beug, H. (2003). Diverse cellular and molecular mechanisms contribute to epithelial plasticity and metastasis. *Nat. Rev. Mol. Cell Biol.* **4**, 657-665.

Halstead, J. M., Lionnet, T., Wilbertz, J. H., Wippich, F., Ephrussi, A., Singer, R. H. and Chao, J. A. (2015). Translation. An RNA biosensor for imaging the first round of translation from single cells to living animals. *Science* **347**, 1367-1671.

Hegerfeldt, Y., Tusch, M., Bröcker, E. B. and Friedl, P. (2002). Collective cell movement in primary melanoma explants: plasticity of cell-cell interaction, beta1-integrin function, and migration strategies. *Cancer Res.* **62**, 2125-2130.

Huot, M.-E., Brown, C. M., Lamarche-Vane, N. and Richard, S. (2009a). An adaptor role for cytoplasmic Sam68 in modulating Src activity during cell polarization. *Mol. Cell. Biol.* **29**, 1933-1943.

Huot, M.-E., Vogel, G. and Richard, S. (2009b). Identification of a Sam68 ribonucleoprotein complex regulated by epidermal growth factor. *J. Biol. Chem.* **284**, 31903-31913.

Klein, M. E., Younts, T. J., Castillo, P. E. and Jordan, B. A. (2013). RNA-binding protein Sam68 controls synapse number and local beta-actin mRNA metabolism in dendrites. *Proc. Natl. Acad. Sci. USA* **110**, 3125-3130.

Kopfstein, L. and Christofori, G. (2006). Metastasis: cell-autonomous mechanisms versus contributions by the tumor microenvironment. *Cell. Mol. Life Sci.* **63**, 449-468.

Lander, R., Nordin, K. and LaBonne, C. (2011). The F-box protein Ppa is a common regulator of core EMT factors Twist, Snail, Slug, and Sip1. *J. Cell Biol.* **194**, 17-25.

Lukong, K. E., Larocque, D., Tyner, A. L. and Richard, S. (2005). Tyrosine phosphorylation of sam68 by breast tumor kinase regulates intranuclear localization and cell cycle progression. *J. Biol. Chem.* **280**, 38639-38647.

Mani, S. A., Guo, W., Liao, M.-J., Eaton, E. N., Ayyanan, A., Zhou, A. Y., Brooks, M., Reinhard, F., Zhang, C. C., Shipitsin, M. et al. (2008). The epithelial-mesenchymal transition generates cells with properties of stem cells. *Cell* **133**, 704-715.

Mardakheh, F. K., Paul, A., Kümper, S., Sadok, A., Paterson, H., McCarthy, A., Yuan, Y. and Marshall, C. J. (2015). Global analysis of mRNA, translation, and protein localization: local translation is a key regulator of cell protrusions. *Dev. Cell* **35**, 344-357.

Mazroui, R., Huot, M.-E., Tremblay, S., Filion, C., Labelle, Y. and Khandjian, E. W. (2002). Trapping of messenger RNA by Fragile X Mental Retardation protein into cytoplasmic granules induces translation repression. *Hum. Mol. Genet.* **11**, 3007-3017.

Miettinen, P. J., Ebner, R., Lopez, A. R. and Derynck, R. (1994). TGF-beta induced transdifferentiation of mammary epithelial cells to mesenchymal cells: involvement of type I receptors. *J. Cell Biol.* **127**, 2021-2036.

Ngan, E., Northey, J. J., Brown, C. M., Ursini-Siegel, J. and Siegel, P. M. (2013). A complex containing LPP and alpha-actinin mediates TGFbeta-induced migration and invasion of ErbB2-expressing breast cancer cells. *J. Cell Sci.* **126**, 1981-1991.

Northey, J. J., Chmielecki, J., Ngan, E., Russo, C., Annis, M. G., Muller, W. J. and Siegel, P. M. (2008). Signaling through ShcA is required for transforming growth factor beta- and Neu/ErbB-2-induced breast cancer cell motility and invasion. *Mol. Cell. Biol.* **28**, 3162-3176.

Paňkova, K., Rösel, D., Novotný, M. and Brábek, J. (2010). The molecular mechanisms of transition between mesenchymal and amoeboid invasiveness in tumor cells. *Cell. Mol. Life Sci.* **67**, 63-71.

Parri, M., Taddei, M. L., Bianchini, F., Calorini, L. and Chiarugi, P. (2009). EphA2 reexpression prompts invasion of melanoma cells shifting from mesenchymal to amoeboid-like motility style. *Cancer Res.* **69**, 2072-2081.

Pinner, S. and Sahai, E. (2008). PDK1 regulates cancer cell motility by antagonising inhibition of ROCK1 by RhoE. *Nat. Cell Biol.* **10**, 127-137.

Sahai, E. and Marshall, C. J. (2003). Differing modes of tumour cell invasion have distinct requirements for Rho/ROCK signalling and extracellular proteolysis. *Nat. Cell Biol.* **5**, 711-719.

Sanz-Moreno, V., Gadea, G., Ahn, J., Paterson, H., Marra, P., Pinner, S., Sahai, E. and Marshall, C. J. (2008). Rac activation and inactivation control plasticity of tumor cell movement. *Cell* **135**, 510-523.

Schmidt, E. K., Clavarino, G., Ceppi, M. and Pierre, P. (2009). SUnSET, a nonradioactive method to monitor protein synthesis. *Nat. Methods* **6**, 275-277.

Serrels, B., Serrels, A., Brunton, V. G., Holt, M., McLean, G. W., Gray, C. H., Jones, G. E. and Frame, M. C. (2007). Focal adhesion kinase controls actin assembly via a FERM-mediated interaction with the Arp2/3 complex. *Nat. Cell Biol.* **9**, 1046-1056.

Taddei, M. L., Giannoni, E., Comito, G. and Chiarugi, P. (2013). Microenvironment and tumor cell plasticity: an easy way out. *Cancer Lett.* **341**, 80-96.

Taddei, M. L., Giannoni, E., Morandi, A., Ippolito, L., Ramazzotti, M., Callari, M., Gandellini, P. and Chiarugi, P. (2014). Mesenchymal to amoeboid transition is associated with stem-like features of melanoma cells. *Cell Commun. Signal.* **12**, 24.

Thiery, J. P., Acloque, H., Huang, R. Y. J. and Nieto, M. A. (2009). Epithelial-mesenchymal transitions in development and disease. *Cell* **139**, 871-890.

Vial, E., Sahai, E. and Marshall, C. J. (2003). ERK-MAPK signaling coordinately regulates activity of Rac1 and RhoA for tumor cell motility. *Cancer Cell* **4**, 67-79.

Wilkinson, S., Paterson, H. F. and Marshall, C. J. (2005). Cdc42-MRCK and Rho-ROCK signalling cooperate in myosin phosphorylation and cell invasion. *Nat. Cell Biol.* **7**, 255-261.

Wolf, K., Mazo, I., Leung, H., Engelke, K., von Andrian, U. H., Deryugina, E. I., Strongin, A. Y., Bröcker, E.-B. and Friedl, P. (2003). Compensation mechanism in tumor cell migration: mesenchymal-amoeboid transition after blocking of pericellular proteolysis. *J. Cell Biol.* **160**, 267-277.

Yamazaki, D., Kurisu, S. and Takenawa, T. (2005). Regulation of cancer cell motility through actin reorganization. *Cancer Sci.* **96**, 379-386.

Yang, J., Mani, S. A., Donaher, J. L., Ramaswamy, S., Itzykson, R. A., Come, C., Savagner, P., Gitelman, I., Richardson, A. and Weinberg, R. A. (2004). Twist, a master regulator of morphogenesis, plays an essential role in tumor metastasis. *Cell* **117**, 927-939.

Zhang, P., Abdelmohsen, K., Liu, Y., Tominaga-Yamanaka, K., Yoon, J.-H., Ioannis, G., Martindale, J. L., Zhang, Y., Becker, K. G., Yang, I. H. et al. (2015). Novel RNA- and FMRP-binding protein TRF2-S regulates axonal mRNA transport and presynaptic plasticity. *Nat. Commun.* **6**, 8888.